Toward a fully automatic left ventricle segmentation using cine-MR images

Isabela Silva[1,2,3], João Sanches[2,3] and Ana G. Almeida[4]

***Abstract*—*Left ventricle* (LV) function is assessed by manually segmenting short axis cardiac *cine magnetic resonance* (cine-MR) images. It is a labor, time-consuming, operator biased task. A series of difficulties arise from these images, that make automatic segmentation of the LV a challenging task: (i) misalignment of the LV along the stack, (ii) signal intensity variation over the stack and over the slice and (iii) the presence of papillary muscles.**

In this thesis, the first steps toward a full automatic LV segmentation algorithm based on a single view of the LV are presented:

1) **Automatic crop: selects a sub-volume containing the LV in all images and in all temporal frames from the acquired data. It is based on three assumptions: (i) the LV is close of the center of the image, (ii) the LV is circular shaped and (iii) there is a high temporal variability of the image intensity in the myocardium boundaries due the heart beat.**
2) **Alignment-by-reconstruction: novel technique to solve the misalignment due to respiratory motion, inspired on the work from Sanches *et al.* [1] in ultrasound;**
3) **Segmentation: the LV is segmented using active contours in an energy minimization formulation with *gradient vector flow* (GVF) as external field. The automatic initialization algorithm here implemented is original, and it is based on the property of intersecting chords.**

Preliminary tests with synthetic and real data from 17 patients were performed with successful results.

***Index Terms*—Left ventricle, automatic crop, intra-plane alignment, snake initialization.**

I. Introduction

According to *World Health Organization* (WHO), cardiovascular diseases are the leading cause of death and were responsible for about 30% of all global deaths in 2005 [2].

Attending to these numbers, there is an increasing demand for technology able to provide qualitative and quantitative information about morphology and function of the heart. The available imaging techniques provide 2-D+T and 3-D+T information with continuously increasing spatial and temporal resolution. Therefore, a single cardiac examination can result in a large amount of data. These advances have led to a raising need for efficient algorithms to automate the extraction of clinical relevant parameters.

MR imaging (MRI) is one of the preferred diagnostic techniques due to its high spatial resolution, soft-tissue contrast and non-ionizing imaging technique. Therefore, it is widely used to diagnose several heart pathologies and it is now considered the "*gold standard*" to evaluate the *left ventricle* (LV) function [3]. One of the most meaningful measures of the LV pump function is the *ejection fraction* (EF), a global index of the LV shortening (Eq. 1):

$$EF = \frac{EDV - ESV}{EDV}, \tag{1}$$

where EDV is the *end-diastolic* (ED) volume and ESV the *end-systolic* (ES) volume.

To estimate the EF, the physicians have to manually draw the LV internal contour from a stack of *short-axis* (SA) cine-MR images at the ED and ES phases of the cardiac cycles. The SA stacks are usually composed by 10 up to 16 slices and 15 up to 30 images are acquired per cardiac cycle, corresponding to different phases of this cycle. Manually processing all this vast amount of data is time consuming, subjective and compromises the accuracy and reproducibility of the quantitative measurements. Therefore, computer assistance is needed.

However, a series of difficulties arise from these SA cine-MR images, that make automatic segmentation of the LV a challenging task:

1) During suspended respiration, there is a displacement of the diaphragm and the heart does not return to the same position on consecutive heart beats [4]. Additionally, the initial position of the diaphragm might change over all the requested apnea periods [4,5]. This can lead to blurring effects and misalignment of the LV along the stack.
2) These images present signal intensity variation: (i) over the stack due to different sensitivity along the coil; (ii) and over the slice due to cardiac flow dynamics [6]. This makes tissue classification with low-level image processing techniques a non-trivial task.
3) Normally, the number of slices acquired exceeds the size of the LV. Physicians are trained to draw contours while at least 50% of the blood pool is surounded by myocardium in both ED and ES [7]. The apical slice is defined as the final slice showing intracavity blood pool at both ED and ES. *Papillary muscles* (PM) are to be included in the volume calculations. This makes manual delineation prone to inter- and intra-observer variability, highly dependant on the physician experience [7].

Due to the stated reasons, there is a growing demand for objective, reproducible and automated technique for quantification of the LV function. However, an infallible automatic segmentation algorithm is now impossible to achieve, therefore the physician will be essential by supervising the outcome and adjusting the result if needed.

Correspondent author: Isabela Silva (isabela.silva@ist.utl.pt).

Thanks to Sociedade Portuguesa de Ressonancia Magnética

Affiliation: [1]Consórcio Engenharia Biomédica; [2]Instituto Superior Técnico, Lisbon, Portugal; [3]Systems and Robotic Institute, Lisbon, Portugal; [4]Faculdade de Medicina da Universidade de Lisboa, Lisbon

II. Problem formulation

LV function is assessed by using SA cine-MR images that represent large amounts of data. Therefore, a reduction of the matrix dimension is needed to reduce the computational burden associated with the pre-processing, alignment and segmentation algorithms required to solve the problems listed above. The development of an automatic crop function suits for a first step in the LV segmentation.

To estimate a ROI containing the LV it is necessary to locate it. In the literature, two different approaches were identified. One is based in the high temporal variability of the image intensity in the myocardium boundaries [8]. The other one uses a size invariant circular *Hough transform* (HT) [9] to locate the LV [10]. The automatic crop algorithm here proposed is based on three assumptions: (i) the LV is close of the center of the image, (ii) the LV is circular shaped and (iii) there is a high temporal variability of the image intensity in the myocardium boundaries due the heart beat.

The second problem to be addressed is misalignment of the LV along the stack. The alignment of the cardiac planes is a non-trivial registration task because there is no rigid-body transformation that gives the minimal energy between the different planes. The problem here is to align a set of misaligned consecutive anatomic planes instead of registering different views of the same object (see Fig. 1). The use of mutual information itself, used in the registration of images from different imaging modalities [11] or to build statistical models [12], is not the most adequate method to solve this problem. Here, a joint image registration and volume reconstruction is proposed, inspired on the previous work from Sanches *et al.* [1] in ultrasound. It is the second step of the algorithm, preceding the segmentation. This is essential to be able to use the initialization of the snake in one slice on the consecutive ones.

After the alignment, the segmentation is finally performed.

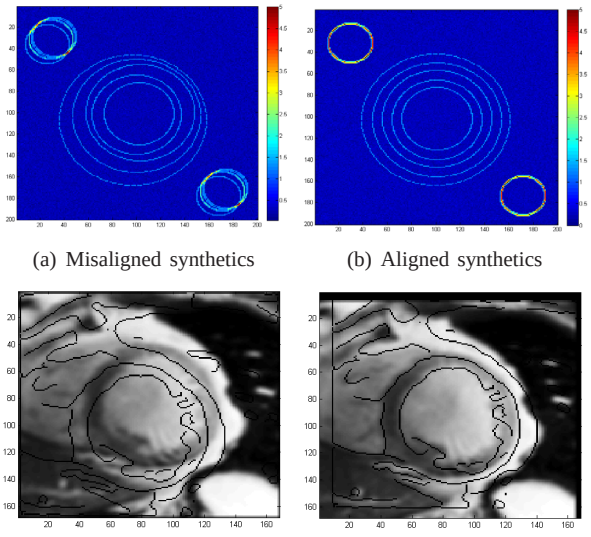

(a) Misaligned synthetics (b) Aligned synthetics

(c) Misaligned real image (d) Aligned real image

Fig. 1. Misalignment in cardiac images: example with synthetics and real images

The LV is segmented using active contours in an energy minimization formulation with GVF as external field. The automatic initialization algorithm here implemented is original, and it is based on the property of intersecting chords.

The Fig. 2 presents the work flow of the solution here proposed.

A. MRI data

The presented algorithm was tested on 17 cardiac patients identified with the letters from A to Q from *Sociedade Portuguesa de Ressonância Magnética* (SPRM) where the LV function was studied. Prof. Ana G. Almeida was the physician in charge, who also validated the obtained results. The images were acquired on a 3T Philips scanner, using a Philips SENSE cardiac coil six-elements and saved in DICOM format (*Digital Imaging and Communications in Medicine*). The cine-MR study was gated to the *electrocardiogram* (ECG) and acquired with steady state free precession imaging sequence.

B. Notation

Over the report, the notations used to access the 3-D+T data-set are listed in the table bellow:

TABLE I
3-D+T NOTATION

Notation	Description
(i, j)	Pixel coordinates, $1 < i, j < M, N$
$[M, N]$	Image size
(i, j, s, t)	Voxel coordinates, $1 < i, j, s, t < M, N, S, T$
s	Slice index, $1 < s < S$
t	Time frame index, $1 < t < T$
$[M, N, S, T]$	Data-set dimensions

III. Automatic crop

The algorithm was implemented by estimating the center of a fixed-size predefined width ROI based on the circular HT. This ROI is then extended to the entire stack of images over all the cardiac cycle frames, resulting in a 3-D+T cropped image volume.

A *standard deviation* (STD) map is computed according to Eq.2, using all temporal slices from the middle plane of the SA images stack. As [8] suggested, high STD is found between the myocardium and the blood-pool. Additionally, this map will introduce extra ringing around the LV borders, i.e., more circular shapes. Therefore, the *a priori* knowledge of the circular shape is used to locate the LV in the STD map using the HT.

$$STD(i,j) = \sqrt{\frac{1}{T}\sum_{t}\left(x\left(i,j,\frac{S}{2},t\right) - \mu_t\left(i,j,\frac{S}{2}\right)\right)^2} \quad (2)$$

Before calculating the STD map, the images are filtered by a Gaussian mask to reduce the noise. This reduction is important guarantee that the STD map observed is mainly generated by

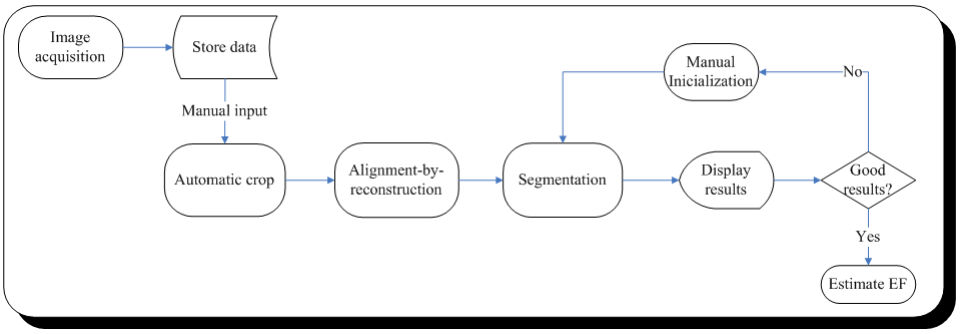

Fig. 2. Algorithm setup

temporal variations and not by spatial noise. The Canny edge-detector [13] is used over the STD map to get an edge-map to be used in the circular HT algorithm.

The circular HT algorithm here implemented[1] is computed for a fixed radius and the output is an accumulator $\mathbf{Acc}$ with the same dimensions of the input image $[M, N]$. The value at $Acc_r(i, j)$ represents the number of circles with radius r centered at the edge pixels that intersect the $(i, j)^{th}$ pixel.

Based on the knowledge that the LV centroid is the center of multiple circles (the ring generated in the STD map and of the epicardial and endocardial border) and that the LV has variable size, the HT is computed for a set of different radius values. The maximum radius of the LV (at the end of the diastole) can range from 18mm to 28mm [14]. Using this interval as reference, the HT was calculated for radius ranging from 15mm to 40mm . The maximum radius was increased to 40mm in order to include the epicardial border of the LV, and the minimum was decreased to 15mm because the middle plane of the stack might not correspond to the largest section of the LV. With steps of 2mm of interval, the circular HT is processed for all the radius from 15mm to 40mm and the accumulators are added at each step (Eq.3). The $\mathbf{Acc}_{Total}$ incorporates the whole information about circles with every radius in the range, amplifying its common center location. Adding the accumulators will ensure that the maximum will be closer to the centroid of the LV.

$$Acc_{Total}(i, j) = \sum_r Acc_r(i, j) \tag{3}$$

Based on the assumption that the LV is always close to the center of the image, the circles detected close to it will be favored. The $\mathbf{Acc}_{Total}$ is then multiplied by a mask that has unitary value in a circular region around the center of the image and with decreasing values up to the borders, following Eq.4.

$$h(\mathbf{x}) = \begin{cases} 1 & \text{if } \|\mathbf{x}-\mathbf{c}\| \leq R \\ \left(\frac{1}{\|\mathbf{x}-\mathbf{c}\|} - \frac{1}{\|\mathbf{c}\|}\right) \cdot R & \text{if } \|\mathbf{x}-\mathbf{c}\| > R \end{cases} \tag{4}$$

where $\mathbf{c} \in R^2$ represents the center of the image, $\mathbf{x} \in R^2$ the position of a mask element and $R = 50$mm, related with human anatomy. This value is fixed and was selected based on experimental tests and on the results from [6]. This reference radius determines the maximum possible distance from which the LV centroid is apart from the center of the image and the circular region where the $\mathbf{Acc}_{Total}$ has unitary weight. Outside this region the $\mathbf{Acc}_{Total}$ is weighted by smaller values, reducing the importance of the detected circles in this area. The mask is zero at the corners of the image. The new ROI is squared and centered at the coordinates of the maximum of the $\mathbf{Acc}_{Total}$. The side dimensions of this *bounding box* (BB) were set to $(2+\epsilon)r_{max} = 120$ mm, where $\epsilon = 1$ is a safety coefficient and $r_{max} = 40$ mm.

[1]"Circle detection via standard Hough Transform" from Amin Sarafraz, downloaded from Matlab Central http://www.mathworks.com/matlabcentral/fileexchange/

IV. Alignment-by-reconstruction

Let $\mathbf{Y}_t^k$ be the edge map of the volume data set of the t^{th} time frame, at the k^{th} iteration step of the algorithm and $\mathbf{Y}(i, j, s)$ be the $(i, j)^{th}$ voxel in the s^{th} slice, where $1 < i, j, s < M, N, S$:

1) Pre-processing: normalization, histogram equalization, power-law transform $\mathbf{I}' = \kappa\mathbf{I}^\gamma$ (where $\kappa = 10$ and $\alpha = 1.3$ to enhance contrast), median filtering and Canny edge detector;
2) Filter $\mathbf{Y_t^k}$ with a broad Gaussian mask to diffuse the contour information;
3) First alignment task: the translation vector T_1 is estimated by calculating the cross-correlation between consecutive planes of the volume and its average subtracted according to Eq.5: let $\mathbf{Y}(\mathbf{x}) = \mathbf{Y}(i, j)$,

$$\mathbf{x}^{k+1}(s) = \mathbf{x}^k(s) + T_1^k(s) - \frac{1}{S}\sum_s^S T_1^k(s). \tag{5}$$

4) Recontruction: The previously aligned set of planes $\mathbf{Y}^0_{IntraPlanesAlignedT_1}$ is used to reconstructed the volume $\mathbf{F}^0$. The reconstruction is an iterative process where the following energy function is minimized:

$$\mathbf{E} = \sum_{i,j,s}^{M,N,S} (\mathbf{F}_{i,j,s} - \mathbf{Y}_{i,j,s})^2 + \alpha \sum_{i,j,s,\delta}^{M,N,S,N_b} (\mathbf{F}_{i,j,s} - \mathbf{F}_{i,j,s,\delta})^2, \tag{6}$$

where N_b is the number of neighbors of each voxel and $\mathbf{F}$ is the unknown volume computed from the original data $\mathbf{Y}$ and influenced by its volume neighbors δ with

and weighting factor α. To compute the minimizer of $\mathbf{E}$, $\mathbf{F}$, Eq.6 must be derived and equal to zero:

$$\frac{\partial \mathbf{E}}{\partial \mathbf{F}_{i,j,s}} = (\mathbf{F}_{i,j,s} - \mathbf{Y}_{i,j,s}) + \alpha N_b \left(\mathbf{F}_{i,j,s} - \bar{\mathbf{F}}_{i,j,s}\right) = 0, \tag{7}$$

$$\text{where } \bar{\mathbf{F}}_{i,j,s} = \frac{1}{N_b} \sum_{\delta}^{N_b} \mathbf{F}_{i,j,s}.$$

To find the solution for this energy minimization, the Newton-Raphson method is used: let $\mathbf{F}_l^k$ be the l^{th} iteration step to estimate $\mathbf{F}^k$,

$$\mathbf{F}_{l+1}^k(i,j,s) = (1+K)\mathbf{Y}^k(i,j,s) + K\bar{\mathbf{F}}_l^k(i,j,s), \tag{8}$$

$$\text{where } K = \frac{\alpha N_b}{1+\alpha N_b}.$$

This is an iterative process, initialized with $\mathbf{F}^0 = \mathbf{Y}$, $\alpha = 0.9$ and $N_b = 6$, and with the stop criterion:

$$\frac{\left\|\mathbf{F}_{l+1}^k - \mathbf{F}_l^k\right\|}{\left\|\mathbf{F}_{l+1}^k\right\|} < 0.1 \tag{9}$$

5) Second alignment task: the translation vector T_2 is estimated by calculating the cross-correlation between the reconstructed and the original planes of the volume and its average subtracted according to Eq.5.

This iterative process stops when T_2 reaches the equilibrium:

$$\frac{\Delta^k}{\Delta^{k-1}} < 0.1, \text{ where } \Delta^k = \left\| \sum_{s}^{S} \left| \bar{T}_2^k(s) - \bar{T}_2^{k-1}(s) \right| \right\| \tag{10}$$

The figure bellow illustrates the algorithm work flow:

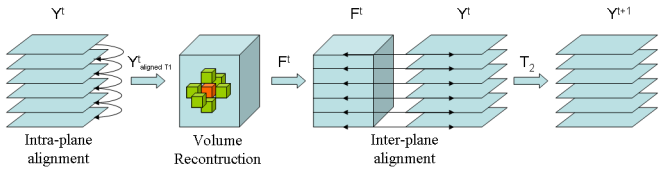

Fig. 3. Alignment-by-reconstruction algorithm

V. Segmentation

To perform the segmentation task, the 2-D formulation of the deformable models will be used, also known as *snakes* or *active contours*. The problem is going to be formulated in terms of the parametric model and in the energy minimization framework.

The parametric active contour is a curve $\mathbf{C}(s) = (\mathbf{x}(s), \mathbf{y}(s))$, $s \in [0,1]$, which moves through the spatial domain of an image to minimize the energy functional from Eq. 11:

$$\mathbf{E}(\mathbf{C}) = \int_0^1 \alpha(s) \left|\frac{\partial \mathbf{C}}{\partial s}\right|^2 + \beta(s) \left|\frac{\partial^2 \mathbf{C}}{\partial s^2}\right|^2 ds + \\ + \int_0^1 \mathbf{P}(\mathbf{C}) ds. \tag{11}$$

The first integral corresponds to the internal energy, the regularization term and second to the potential energy. Typically, the potential function is based on the gradient of the image: given a gray-level image $\mathbf{I} : R^2 \to R$, viewed as a function of continuous positions variables, a typical potential energy function designed in such a way that intensity transitions become associated to valleys of the potential is

$$\mathbf{P}(x,y) = -w_e \left|\nabla[\mathbf{G}_\sigma(x,y) * \mathbf{I}(x,y)]\right|^2, \tag{12}$$

where w_e is a positive weighting factor, $\mathbf{G}_\sigma(x,y)$ is a 2-D Gaussian function with standard deviation σ, ∇ is the gradient operator and $*$ is the 2-D convolution operator.

The problem of finding a curve $\mathbf{C}(s)$ that minimizes the energy functional E (Eq. 11) is known as variational problem. The curve that minimizes $\mathbf{E}$ must satisfy the following Euler-Lagrange equation Eq. 13a, that can also be analyzed as a force balance equation Eq. 13b.

$$\frac{\partial}{\partial s}\left(\alpha \frac{\partial \mathbf{C}}{\partial s}\right) - \frac{\partial^2}{\partial s^2}\left(\beta \frac{\partial^2 \mathbf{C}}{\partial s^2}\right) - \nabla \mathbf{P}(\mathbf{C}) = 0. \tag{13a}$$

$$\mathbf{F}_{int}(\mathbf{C}) + \mathbf{F}_{pot}(\mathbf{C}) = 0. \tag{13b}$$

To find the object boundary, parametric curves are initialized within the image domain (manually or automatically), and are forced to move toward the potential energy minima under the influence of both these forces. To find the solution to Eq. 13a, the active contour is made dynamic by treating $\mathbf{C}(s)$ as a function of time $t \to \mathbf{C}(s,t)$. The time zero contour, $\mathbf{C}(s,0)$, is given by the initialization contour. Then the snake evolves iteratively according to Eq. 14:

$$\frac{\partial \mathbf{C}}{\partial t} = \mathbf{F}_{int}(\mathbf{C}) + \mathbf{F}_{pot}(\mathbf{C}). \tag{14}$$

The main advantages of the snakes are their ability to generate a parametric and smooth curve from the image. However, most of the active contour models are sensitive to noise due to their purely edge-based nature and low attraction range of the gradient. For this reason it will be implemented the *gradient vector flow* (GVF) presented by Xu and Prince [15] and an automatic initialization algorithm as well.

A. Gradient Vector Flow

Let $f : R^2 \to R$ be the edge map derived from the image $\mathbf{I}$ and $\mathbf{F}_{pot}(x,y) = \mathbf{v}(x,y) = [u(x,y), v(x,y)]$ be the GVF field that minimizes the energy functional from Eq. 15:

$$\epsilon = \iint \mu(u_x^2 + u_y^2 + v_x^2 + v_y^2) + |\nabla f|^2 |\mathbf{v} - \nabla f|^2) dxdy. \tag{15}$$

The edge map $f(x,y)$ has three general properties: (i) the gradient of an edge map ∇f has vectors pointing toward the edges, (ii) these vectors generally have large magnitudes only in the vicinity of the edges, and (iii) in homogeneous regions, where $\mathbf{I}(x,y)$ is nearly constant, ∇f is nearly zero.

According to f properties, the variational formulation in Eq. 15 makes the result smooth when the region is homogeneous. In particular, when $|\nabla f|$ is small, the energy is dominated by the partial derivatives of the vector field. On the other hand, when $|\nabla f|$ is large, the second term dominates the integrand and is minimized by setting $\mathbf{v} = |\nabla f|$. The parameter μ is a regularization parameter and should be set according to the amount of noise present in the image.

Euler equations are again used to solve this variational problem and calculate the GVF field:

$$\mu\nabla^2 u - (u - f_x)(f_x^2 + f_y^2) = 0 \quad (16a)$$
$$\mu\nabla^2 v - (v - f_y)(f_x^2 + f_y^2) = 0 \quad (16b)$$

where ∇^2 is the Laplacian operator.

B. Automatic snake initialization

The snake initialization is a very important step in segmentation, determinant for a good convergence.

LV imaging has special characteristics that make this issue important. In one hand, edge detectors are not able to fully detect the endocardium border without detecting other spurious structures as well. These noisy structures present in the blood pool have contrast transitions close to some weak edges (compare Canny performance for different thresholds in Fig.4) and are generated by turbulent blood-flow.

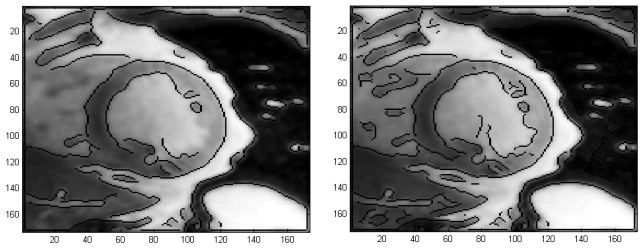

(a) Weak edges, Canny default (b) Spurious edges, Canny 0.01 - 0.1 threshold

Fig. 4. Weak edges in cine-MR images using Canny edge-detector. The dark lines represent the edges over the original image

On the other hand, HT does not give a satisfying center/radius estimation to initialize the contour with a circumference based on those parameters. It is a very sensitive system, and the circumference can fall out of the borders and compromise the convergence of the contour leading to a mixed epicardium-endocardium final contour or be stuck in the spurious structures such as PM.

Our approach is robust to all the difficulties in LV segmentation because is based on the gray-scale image and not on the edge-map. The only request is that the center of the image must be inside the blood-pool, which is accomplished in section **??**. Inspired from [16], the property of intersecting chords is used, where the perpendicular bisector of any chord passes through the center of the circumference.

Using two chords, the center can be estimated but with no error associated. Therefore, four chords will be used to estimate more accurately the best circumference center (see Fig.5). The signal profiles from four direction in the image are collected: horizontal, vertical and two diagonals.

C. Implementation

The data-set from the *alignment-by reconstruction* step (the aligned and pre-processed data-set) is the input for this final step. The setup in Fig.6 explains the work flow of this process.

The process starts at the first frame and middle slice, $s = S/2$. The first frame is collected at the QRS complex from

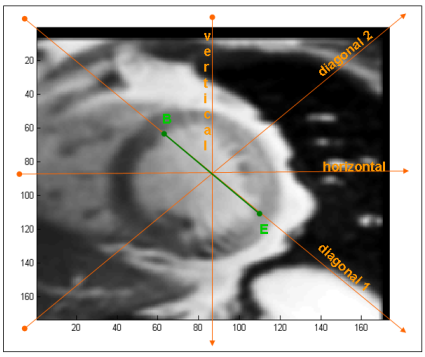

Fig. 5. Signal profile directions collected from the middle plane: the arrows point the way the signal was collected. The points 'B' and 'E' define the chord.

the ECG, that represents the start of the systole, therefore, the end of the diastole. After the initialization, the segmentation algorithm is used and the contour is expanded in space and time through its neighbors, as exemplified in Fig.6(b).

Over the time, the area is measured and the *ES frame* (ESF) is the one with minimum area. It is expected to find the ESF at about 40% of the time course (the systole is shorter then the dyastole [17]) in normal heart-beat conditions. After estimating the ESF, the contour is initialized in the midle slice with the contour from the segmentation of the time series. Then, the contours are again propagated over the space.

After each segmentation step, the results are displayed and can be manually changed. The spurious slices have to be manually excluded.

VI. Results and discussion

LV function is assessed by using SA cardiac cine-MRI that represent large amounts of data: 10 up to 17 volume images over 15 up to 30 frames in the cardiac cycle. This data is inspected manually by the expert and contours are drew manually to extract the EF value. It is a time consuming process and its full automatization is of great interest.

The work here presented describes three automatic first steps toward a full automatization of the LV segmentation in cine-MR images: crop, registration and initialization of the segmentation. The segmentation step itself, based on active contours, still requires human intervention for a satisfying result. The algorithms here proposed was tuned and tested with images acquired from 17 patients identified with letters from A to Q. The most important results from the three steps are summarized in Table II.

Automatic crop

The success of the cropping algorithm depends on whether the BB is able to fully contain the LV. The contents of the estimated BB for all the data-sets were visually inspected for every slice over all time frames. The quantification of the image size reduction is presented in the summary Table II.

All the tested data-sets had successful results, *i.e.*, the LV was always within its borders. Even considering the misalignment between consecutive planes, the LV endocardial and

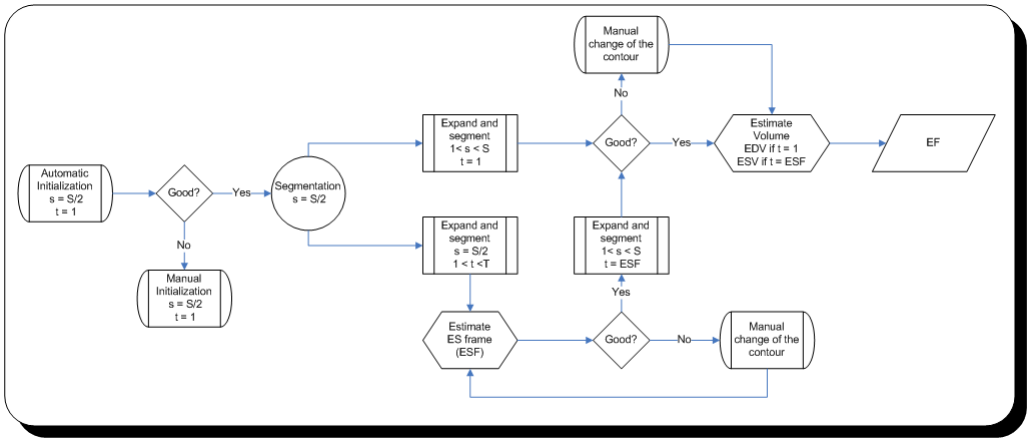

(a) Work flow

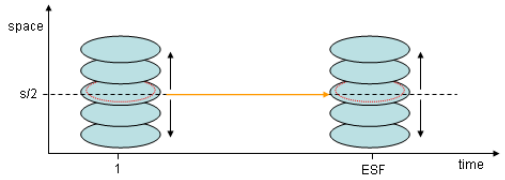

(b) Expansion of the contours in space

Fig. 6. Segmentation work flow.

epicardial borders were always inside the estimated fixed-size window. Here, the reduction only depends on the resolution of the image. In most of the cases, the size of the cropped images is equal to 30.0% of the original image. The biggest reduction was 25.4% with patient J, and the worst case was observed in patient Q, with a reduction to 34.0% of the original size (see Table II).

In Fig.7(a) and Fig.7(b) it is possible to observe the estimated ROI in images with resolutions different from the usual, where the algorithm performed successfully: 672×672 in patient J and 256×256 in patient Q. As previously mentioned, the signal intensity is not constant over the volume due to differences in the sensitivity along the coil and also along the slice due to cardiac flow dynamics [6]. This algorithm proved to be robust to signal variation over the image, which is usually a difficulty that must be dealt with. The proposed algorithm is able to cope with this problem because it does not depend directly on the original image but on the STD map, which decreases its sensitivity to these fluctuations.

Although the algorithm only takes the middle slice to calculate the BB, it has proven to be robust to plane misalignment, mainly because they are usually small and the cropped window is big enough to fit them. It is not, however, able to consistently locate the exact center of the LV because usually it is not a trivial task to define it. This is shown in the results from patient H and I in Fig.7(c) and Fig.7(d) respectively. Although the center was not located successfully, the center of the BB is close enough from the LV centroid and the whole LV is inside the BB. This algorithm located another circular structure close to the LV, like the myocardium that encloses the LV and the right ventricle, who's center is close to the LV. Despite the fact that the whole LV is inside the BB, the LV centroid is slightly away from its center.

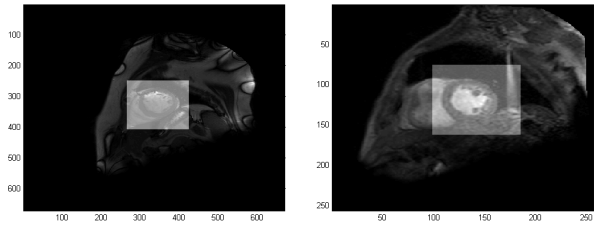

(a) Patient J, resolution 672×672 (b) Patient Q, resolution 256×256

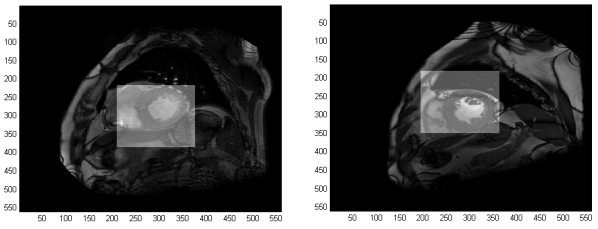

(c) Patient H (d) Patient I

Fig. 7. Automatic crop results

These SA images typically have 560×560 pixels covering a *field of view* (FOV) containing the heart and much more. Reduction of matrix dimension is an important first step to exclude unnecessary information and speed up the processing tasks. In this work it is presented a fully automated crop function that successfully performed this task over the data from 17 patients.

Alignment-by-reconstruction

The alignment of the planes is needed for an efficient segmentation. Here, a method called *alignment-by-reconstruction*

is used, where and intermediate reconstruction step is implemented. Experimental tests were performed with the algorithm here presented: with synthetic and real data.

The synthetic volume has a 5 slices. In each slice there is a central circumference and two smaller circumferences placed perifericaly. The radius of the central circumference increased from plane $1 \rightarrow 5$ and the radius of the smaller ones is fixed. Pseudorandom noise (signal between $[0, 1]$) normally distributed with amplitude of 10% of the signal, *i.e.*, about -10.8dB, was also included.

To simulate the misalignment that can be found in real data, these planes were misaligned with a translation vector randomly generated with normally distributed components (Fig.1(a)), with 0 mean and standard deviation σ. The σ represents how much the plane will be misaligned from its original position.

In order to confirm the importance of the reconstruction, the first synthetic tests missed that step. The synthetic data was misaligned with a fixed translation vector, generated with $\sigma = 3$. The performance of the algorithms was accessed by estimating the error of the translation (Eq.17). With $\alpha = 1.5$, the translation error for the algorithm without reconstruction was 3.2, while the error with the reconstruction step was 0.4. Comparing the translation errors, it is clear that the reconstruction step is essential. The importance of the reconstruction step is based on the information that each plane incorporates about its neighbors.

$$\|\vec{e}\| = \left\| \frac{1}{S} \sum_{s}^{S} T_{original}(s) + T_{estimated}(s) \right\|. \qquad (17)$$

In what concerns to the real data, the algorithm was tested in 17 cardiac patients. The performance of the algorithm could only be accessed in a qualitative way, by observing the segmentation results where the deformed contour from slice $s = n$ was used to initialize the neighbor planes $s = n + 1$.

The observed results were generally good. The α parameter was set to 0.9 for all patients. Depending on the amount of data (number of slices mainly), the algorithm could require more iteration steps to converge. The time series were also analyzed, where it was observed that there is no misalignment over the time dimension.

Segmentation

After proper tuning of the snake parameters, the data from 17 patients were segmented and manually changed with expert supervision.

Automatic snake initialization: The initialization algorithm was tested over the available patient data. This is the first step where segmentation takes part. Based on the intersecting chords property, a set of points (8 to 16) is estimated and linearly interpolated. This curve with sharp edges (see green dots in Fig.8), is the initialization contour for the *snake deformation*, from the middle slice $s = S/2$ and time frame $t = 1$, corresponding to the ED phase. The initialization is considered good once the myocardium border is segmented with the contour (see the *magenta* line in Fig.8).

Over all the data, the user intervention was most of the times necessary to manually change the automatic initialization contour into a good initialization. In this step, human intervention is essential since the criteria to segment the myocardium are highly experience-dependent specially due to PM.

This algorithm was tested with two values for the maximum length of the chords: 56mm and 65mm. The first one is the double of the normal maximum radius (see section III) and the second is used to include pathological dilated hearts. See summary Table II at the end of this section, the percentage of the segmented contour manually generated.

These two diameters were tested because some difficulties came up, for instance in patients K and N, where the maximum diameter of 56mm was not enough, *i.e.*, there were no sets of chords who fulfilled all the criteria. For this reason, a higher maximum diameter was tested and it performed better in some cases, where probably the heart is dilated. However, in average it performed worse and in two cases the amount of candidate chords caused problems of memory (patients F and O). Therefore, the maximum normal diameter 56mm is the best option.

The best results were observed in patients A, B and D, where human intervention was very small. The PM are responsible for most of the required manual changes (Fig.9(a)). They are small structures located in the blood cavity or in the myocardium borders with the same contrast of the myocardium, therefore, their borders might be better ranked than the points resulting from transitions in the endocardium. However, only an expert is qualified to define where the contour should pass, specially when the PM are in the myocardium border (see Fig.8 to Fig.9 to see different types of PM).

Another problem that affected the performance of the automatic initialization was the centering alteration after the alignment task, presented in Fig.9(b). This happened with the patient K. In this patient, there was no set of initialization points that fulfill the requirements, and therefore the initialization has to be performed completely manually.

For each patient, the segmentation parameters were tunned. Most of the patients could be grouped with similar parameters. The ideal contour estimated from this step is used to initialize the contours for both time and space segmentation, as described in the next sections.

ESF estimation: With the correct setup of the segmentation parameters, the ESF was automatically estimated for most of the patients (9 out of 17). The initialization for the ESV estimation was also estimated in this step, where 7 out of 17 were correctly automatically segmented. The estimated ESF are listed in Table II along with the correct ESF. An example is showed in Fig.10.

Analyzing the results presented in Table II, in most of the cases where the ESF is miss-estimated, the error is normally of 1 time frame (exception for patients N and P).

The segmentation in the time domain is less prone to difficulties since the temporal resolution is generally high and the transition between frames is smooth. However, the PM might introduce error in the ESF estimation or in ESF segmentation and there are difficulties when the cavity at the ESF is very small. Therefore, the expert supervision is very

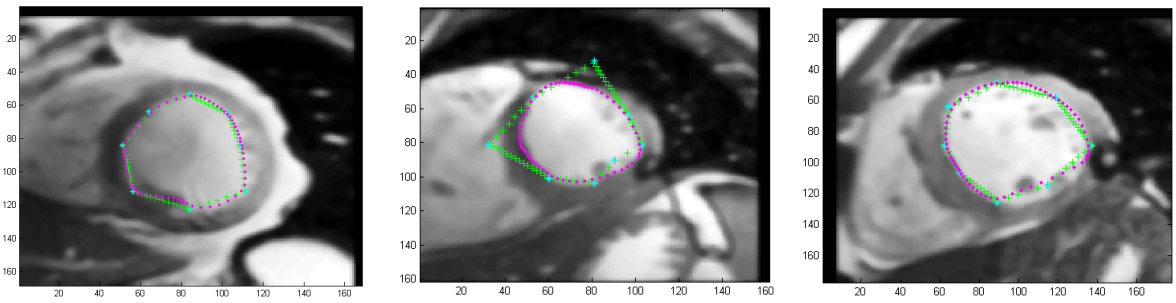

(a) patient A, 22.8% changed (b) patient B, 25.7% changed (c) patient D, 24.6% changed

Fig. 8. Automatic initialization results. (*blue star*) points from intersecting chords (*green cross*) linear interpolation from the beginning points (*magenta dashed*) contour after segmentation algorithm

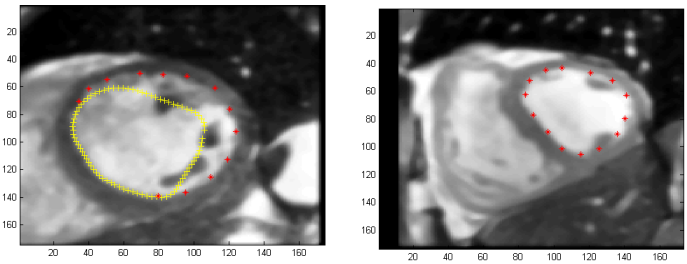

(a) Papillary muscles, patient N (b) Bad centering after alignment, patient L

Fig. 9. Automatic initialization results: difficulties. (*magenta*) contour after segmentation algorithm, (*yellow*) Initialization contour, (*red*) manual changing a segment of the contour.

important.

The segmentation of the time series was also used to prove the hypothesis assumed that the first time frame corresponded to the ED phase. The area of the frame $t = T$ was smaller that $t = 1$ for all the tested patients. Additionally, when the estimated ESF is about half of the time course, it can be an indication for taquicardia.

Snake deformation: In the last step of the segmentation process, the ED and ES volumes are segmented. For every patient, the set of segmentation parameters was tunned in the ED and ES phase. For some patients, the same set was used for both cardiac phases.

Thanks to the alignment step, the contour propagation method worked successfully in most of cases. However, two main difficulties came up: (i) the PM stopped the evolution of the snake into the myocardium and (ii) the abrupt radius variation of the LV section at base and appex did not allowed the use of the neighbor contours in these cases. Fortunately, in most of the cases these are also the disposable slices, where there was no LV left or did not fulfill the criteria to be accounted to the EF estimation (see section I).

In the example presented in the figures Fig.11, the contour propagation in the middle planes is smooth. However, closer to the appical planes the PM increase their influence and the results have to be manually changed.The LV radius decrease from $3 \rightarrow 4$ is high and therefore the segmentation is poorer.

In the presented example, the diastolic slices required no changes in $6, 7$, minor changes in $4, 5$ and major interventions in $1, 2, 3$. The systolic slices required no changes in $3, 6, 7$, minor changes in 4 and major interventions in $1, 2, 5$. Once the segmentation parameters can be automatically setup, these results represent great improvement to the clinical routine, because only minor changes have to be performed.

These results were inspected by an expert and the EF was estimated and compared with the software in the workstation. The main difficulties found in the presented solution concern the user interface, where zooming and contrast change is no option. Therefore, the manual changes introduced have low reproducibility. The software result was $EF = 63\%$ and the presented algorithm showed values between 62% and 67%.

The incorporation of shape information, or the elimination of the PM are the two main steps that follow in order to be less sensitive to the segmentation parameters.

VII. Conclusions

The LV function analysis is currently performed manually in the clinical routine in a labor, time-consuming, operator biased task. In most of the proposed algorithms only a part of the stated difficulties are addressed. According to this lack, a new approach must be used, combining most of the proposed models and methodologies and attending to all the SA cine-MR difficulties in order to achieve an improved, robust and fully automated LV segmentation.

Based on the HT, the *automatic crop* algorithm was able to robustly reduce the image size for all the data tested to about 30% of the original size, reducing the computation burden for the tasks that follow.

The *alignment-by-reconstruction* step had encouraging results with the synthetic data, highlighting the importance of

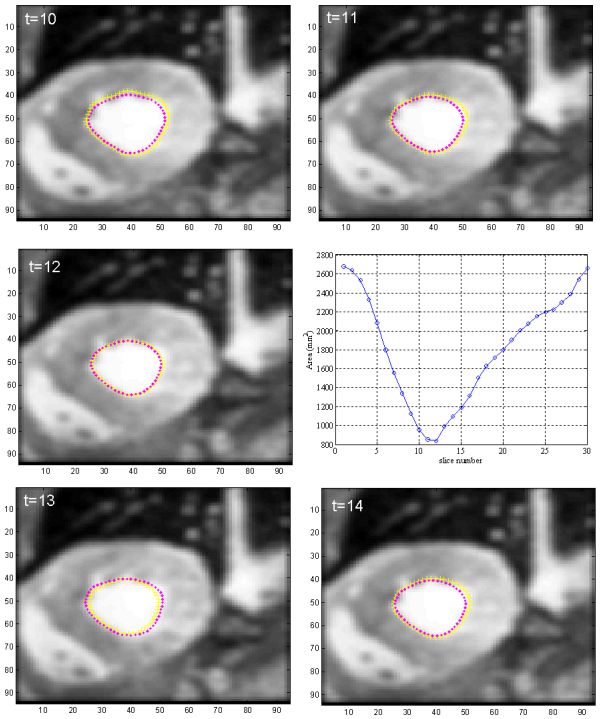

Fig. 10. Segmented time series around the ESF, patient E. (*yellow cross*) linear interpolation from the beginning points (*magenta dashed*) contour after segmentation algorithm (*graphic*) area estimation over all time series.

the reconstruction step. With the real data, the observed results were also important, as they allowed an efficient segmentation.

In what concerns to the segmentation, the *automatic snake initialization* algorithm implemented showed some limitations due to the PM, however represents a refreshing contribution to solve this problem where expert intervention is generally smaller. The ESF was successfully automatically identified in 9 out of 17 patients.

A full volume segmentation is also implemented. The major limitation here is the setup of the segmentation parameters. This difficulty can be overcome with future work, introducing shape information and reducing the importance of the internal forces. However, the importance of this step is to validate the previously described algorithms, that represent a great contribution toward a fully automatic LV segmentation.

TABLE II
SUMMARY OF MAIN RESULTS. (T) WHEN NO INITIALIZATION IS AUTOMATICALLY SUGGESTED. (^{1}) MANUAL IDENTIFICATION OF THE ESF. (^{2}) MANUAL CHANGE OF THE CONTOUR OF THE ESF.

Patient	Crop Reduction	Change Initialization	ESF	
			Est.	Cor.
A	30.0%	22.8%	14	14
B	30.5%	25.7%	7	7
C	30.0%	38.7%	$8^{(1,2)}$	9
D	32.4%	24.6%	14^2	14
E	28.1%	T	12	12
F	30.0%	$(32.7 + 32.9)\%$	$12^{(1,2)}$	13
G	30.0%	$(33.7 + 30.9)\%$	12^2	12
H	30.0%	71.1%	$10^{(1,2)}$	9
I	30.0%	$(49.4 + 18.9)\%$	$12^{(1,2)}$	13
J	25.4%	32.1%	14	14
K	26.3%	T	13^2	13
L	30.0%	62.8%	13	13
M	30.0%	48.8%	10	10
N	30.0%	T	$8^{(1,2)}$	13
O	30.2%	64.9%	9	9
P	30.0%	53.6%	$13^{(1,2)}$	15
Q	34.0%	71.1%	$12^{(1,2)}$	12
Mean $\pm$ STD	29.8 ± 1.9	55.5 ± 29.0		

REFERENCES

[1] J. Sanches and J. S. Marques, "Joint image registration and volume reconstruction for 3d ultrasound," *Pattern Recognition Letters*, vol. 24, pp. 791–800, 2003.

[2] WHO, "Cardiovascular diseases, fact sheet nr. 137," Online, World Health Organization, February 2007.

[3] i. c. w. t. a. o. e. P. c. Task force of the European Society of cardiology, "The clinical role of magnetic resonance in cardiovascular disease," *European Heart Journal*, vol. 19, pp. 19–39, 1998.

[4] A. Holland, J. Goldfarb, and R. Edelman, "Diaphragmatic and cardiac motion during suspended breathing: preliminary experience and implications for breath–hold mr imaging," *Radiology*, vol. 209, no. 2, pp. 483–489, November 1998.

[5] K. McLeish, D. Hill, D. Atkinson, J. Blackall, and R. Razavi, "A study of the motion and deformation of the heart due to respiration," *Medical Imaging, IEEE Transactions on*, vol. 21, no. 9, pp. 1142–1150, Sep 2002.

[6] A. Pednekar, R. Muthupillai, V. Lenge, I. Kakadiaris, and S. Flamm, "Automatic identification of the left ventricle in cardiac cine-mr images: Dual-contrast cluster analysis and scout-geometry approaches," *Journal of Magnetic Resonance Imaging*, vol. 23, pp. 641–651, April 2006.

[7] T. D. Karamitsos, L. E. Hudsmith, J. B. Selvanayagam, S. Neubauer, and J. M. Francis, "Operator induced variability in left ventricular measurements with cardiovascular magnetic resonance is improved after training," *Journal of Cardiovascular Magnetic Resonance*, vol. 9, no. 5, pp. 777–783, September 2007.

[8] C. A. Cocosco, T. Netsch, J. Sénégas, D. Bystrov, W. J. Niessen, and M. A. Viergever, "Automatic cardiac region-of-interest computation in cine 3d structural mri," *CARS*, pp. 1126–1131, 2004.

[9] D. H. Ballard, "Generalizing the hough transform to detect arbitrary shapes," *Pattern Recognition*, vol. 13, no. 2, pp. 111–122, 1981.

[10] A. Müller, A. Neitmann, N. Merkle, J. Wohrle, V. Hombach, and H. Kestler, "Contour detection of short axis slice mr images for contraction irregularity assessment," *Computers in Cardiology*, pp. 21–24, 2005.

[11] T. Makela, P. Clarysse, O. Sipila, N. Pauna, Q. C. Pham, T. Katila, and I. E. Magnin, "A review of cardiac image registration methods," *IEEE Transactions on Medical Imaging*, vol. 21, no. 9, pp. 1011–1021, September 2002.

[12] A. F. Frangi, D. Rueckert, J. A. Schnabel, and W. J. Niessen, "Automatic construction of multiple-object three-dimensional statistical shape models: application to cardiac modeling," *IEEE Transactions on Medical Imaging*, vol. 21, no. 9, pp. 1151–1166, September 2002.

[13] J. Canny, "A computational approach to edge detection," *Pattern Analysis and Machine Intelligence, IEEE Transactions on*, vol. PAMI-8, no. 6, November 1986.

[14] H. Feigenbaum, *Feigenbaum's echocardiography*. Philadelphia: PA: Lippincott, 2005.

[15] C. Xu and J. L. Prince, "Snakes, shapes, and gradient vector flow," *IEEE Transactions on Image Processing*, vol. 7, no. 3, pp. 359–369, March 1998.

[16] H.-S. Kim and J.-H. Kim, "A two-step circle detection algorithm from the intersecting chords," *Pattern Recognition Letters*, vol. 22, pp. 787–798, 2001.

[17] W. F. Ganong, "The heart as a pump," in *Review of Medical Physiology (LANGE Basic Science)*, 20^{th} *edition*, J. M. Fitzpatrick and M. Sonka, Eds. McGraw-Hill Medical, 2001.

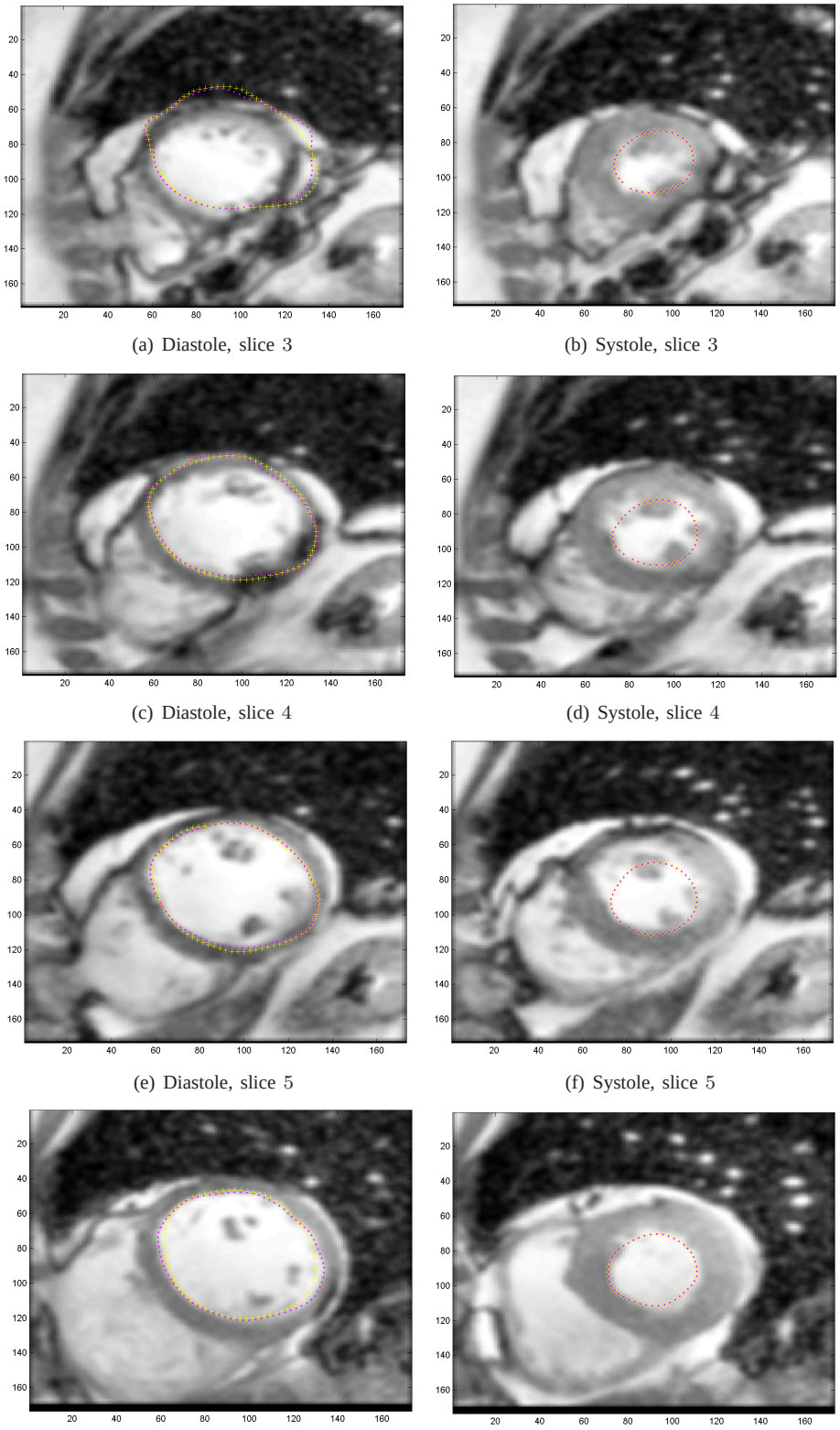

(a) Diastole, slice 3 (b) Systole, slice 3

(c) Diastole, slice 4 (d) Systole, slice 4

(e) Diastole, slice 5 (f) Systole, slice 5

(g) Diastole, slice 6 (h) Systole, slice 6

Fig. 11. Segmentation results, plane 3 to 6, patient G. (*magenta*) contour after segmentation algorithm, (*yellow*) Initialization contour.